**Supporting Information for**

# Insights into the Influence of Support and Potassium or Sulfur Promoter on Iron-based Fischer-Tropsch Synthesis: Understanding the Control of Catalytic Activity, Selectivity of Lower Olefins, and Catalyst deactivation

Feng Jiang†, Min Zhang†, Bing Liu, Yuebing Xu, and Xiaohao Liu*

*Department of Chemical Engineering, School of Chemical and Material Engineering, Jiangnan University, 214122 Wuxi, China*

* *Corresponding author. E-mail address: liuxh@jiangnan.edu.cn (X.H. Liu)*

† *The authors contributed equally to this work.*

## 1. Calculation method for the catalytic performance

The catalytic performance was evaluated in terms of CO conversion and selectivity of hydrocarbons. The total CO conversion $X_{CO}$ was calculated as:

$$X_{CO} = \left(\left(A_{CO}/A_{N_2}\right)_{in} - \left(A_{CO}/A_{N_2}\right)_{out}\right)/\left(A_{CO}/A_{N_2}\right)_{in} \times 100$$

where $\left(A_{CO}/A_{N_2}\right)_{in}$ and $\left(A_{CO}/A_{N_2}\right)_{out}$ are the peak area ratio of CO to $N_2$ at the inlet and outlet of reactor, respectively. The total CO conversion can be devided into $CO_2$ and hydrocarbons. The selectivity of CO converted to $CO_2$ ($S_{CO\ to\ CO_2}$) was calculated as:

$$S_{CO\ to\ CO_2} = \left\{\left(A_{CO_2}/A_{N_2}\right)_{out} \times f_{CO_2}/\left(\left(A_{CO}/A_{N_2}\right)_{in} - \left(A_{CO}/A_{N_2}\right)_{out}\right) \times f_{CO}\right\} \times 100$$

where $\left(A_{CO_2}/A_{N_2}\right)_{out}$ is the peak area ratio of $CO_2$ to $N_2$. $f_{CO_2}$ and $f_{CO}$ are the correction factors of $CO_2$ and CO. The selectivity of CO converted to hydrocarbons ($S_{CO\ to\ HC}$) was calculated as:

$$S_{CO\ to\ HC} = 100 - S_{CO\ to\ CO_2}$$

The selectivity of CO converted to $CH_4$ was calculated as:

$$S_{CO\ to\ CH_4} = \left\{\left(A_{CH_4}/A_{N_2}\right)_{out} \times f_{CH_4} / \left(\left(A_{CO}/A_{N_2}\right)_{in} - \left(A_{CO}/A_{N_2}\right)_{out}\right) \times f_{CO}\right\} \times 100$$

where $S_{CO\ to\ CH_4}$ is the selectivity of $CH_4$ ($CO_2$ included as product). $\left(A_{CH_4}/A_{N_2}\right)_{out}$ is the peak area ratio of $CH_4$ to $N_2$. $f_{CH_4}$ is the correction factor of $CH_4$. Therefore, the selectivity of $CH_4$ in total hydrocarbons ($S_{CH_4\ in\ HC}$) product was calculated as:

$$S_{CH_4\ in\ HC} = S_{CO\ to\ CH_4}/S_{CO\ to\ HC} \times 100$$

The selectivity of hydrocarbons from carbon number *n* to carbon number *n* + *k* ($S_{C_n - C_{n+k}\ in\ HC}$) was calculated as: $S_{C_n\ in\ HC} = S_{CO\ to\ C_n}/S_{CO\ to\ HC} \times 100$

$$S_{C_n - C_{n+k}\ in\ HC} = \sum_{i=n}^{n+k} S_{CO\ to\ C_n}/S_{CO\ to\ HC} \times 100$$

where $S_{C_n\ in\ HC}$ is the selectivity of $C_n$ produced from gas phase and liquid phase products during the stable period.

## 2. Catalyst characterization details

*2.1 BET surface area and pore volume*

The specific surface areas and total pore volume were determined from $N_2$ adsorption/desorption isotherms at -196 °C using an automated surface area and pore size analyzer (Micromeritics ASAP 2020). Prior to the measurement, the sample was degassed at 150 °C for 4 h under vacuum. The specific surface area was determined according to the BET method in the relative pressure range of 0.05-0.3. The pore size and pore volume were calculated based on the Barrett-Joyner-Halenda (BJH) method using the desorption branches of the $N_2$ isotherms.

*2.2 X-ray diffraction*

The powder X-ray diffraction (XRD) patterns were recorded by a Bruker AXS D8 Advance diffractometer using Cu(Kα) radiation (λ = 1.5406 Å) at 40 kV and 40 mA at room temperature (RT)

with 0.02° step size and 0.4 s step time from 5 to 90°. Prior to the characterization of activated samples, the samples were passivated in the flowing gas of $N_2$ (1% $O_2$ in $N_2$) at RT for 1 h The crystallite phases were determined by comparing the diffraction patterns with those in the standard powder XRD files (JCPDS) from the International Center for Diffraction Data.

*2.3 Transmission electron microscopic images*

Transmission electron microscopic (TEM) images of the samples were obtained by using a JEOL JEM-2100 microscope operating at 200 kV. The samples were prepared by dropwise addition of the dilute catalyst suspension on a copper-coated carbon TEM grid followed by the evaporation of the solvent ethanol. The iron particle histograms were obtained via evaluating several hundred detected iron particles from the TEM images.

*2.4 Hydrogen temperature-programmed reduction*

$H_2$ temperature-programmed reduction (TPR) was recorded by an automated chemisorption analyzer (TP5076 TPD/TPR) using a gas chromatograph equipped with a thermal conductivity detector. Typically, prior to the TPR measurements, 50 mg samples were treated at 200 °C in a $N_2$ flow for 1 h to remove traces of water and impurities and then cooled to RT. The gas mixture (5% $H_2$ + 95%$N_2$) flow (30 mL $min^{-1}$) was introduced to the sample bed until a stable baseline was reached. The $H_2$ TPR curve was recorded from 30 to 900 °C at a heating rate of 10 °C $min^{-1}$.

*2.5 Fourier transform infrared spectroscopy*

The Fourier transform infrared spectroscopy (FTIR) spectra were recorded with a Nicolet 6700 FTIR spectrophotometer in the range of approximately 4000-500 $cm^{-1}$ with a resolution of 2 $cm^{-1}$. The specimens for FT-IR measurements were prepared by grinding the samples with KBr together,

and then compressed into thin pellets under 10 MPa.

*2.6 Thermogravimetric analysis*

Thermogravimetric (TG) analysis of the spent and reduced catalysts to determine the properties of carbon deposits was performed on a Mettler-Toledo TGA-1100SF Thermogravimetric analyzer. In TG analysis, 10 mg samples were heated in a flow of pure oxygen (10 mL $min^{-1}$) from 30 to 600 °C at a heating rate of 5 °C $min^{-1}$.

*2.7 Transmission Mössbauer spectrometry*

The Transmission Mössbauer spectrometry (TMS) was carried out to identify the iron-based phases. Transmission $^{57}Fe$ Mössbauer spectra were collected at RT on an MR-351 constant-acceleration Mössbauer spectrometer (FAST, Germany) using a 25 mCi $^{57}Co$ in Pd matrix. The spectrometer was operated in the summetric constant acceleration mode. Data analysis was performed using a nonlinear least-squares fitting routine that models the spectra as a combination of singlets, quadruple doublets, and magnetic sextuplets based on a Lorentzian line shape profile.

*2.8 X-ray photoelectron spectroscopy*

X-ray photoelectron spectra (XPS) spectra were recorded by a Thermo SCIENTIFIC ESCALAB 250xi X-ray photoelectron spectrometer using Al-Kα (1486.8 eV) as the exciting source at 15 kV and 10 mA. The background vacuum of the analysis chamber was $2 \times 10^{-9}$ mbar. The binding energies (BE) were calibrated using the C1s peak at 284.8 eV from adventitious carbon. In experiments, the samples were pressed into self-supported wafers and mounted on the stainless-steel manipulator.

## 3. Computational details

All the density functional theory (DFT) calculations were performed using the All the density functional theory (DFT) calculations were performed using the Vienna *ab initio* simulation package (VASP).[1,2] The projector-augmented wave method was used to represent core-valence interactions.[3] Valence electrons were described by a plane wave basis with an energy cutoff of 400 eV. The generalized gradient approximation with the Perdew-Burke-Ernzerhof functional was used to model electronic exchange and correlation.[4] Gaussian smearing with a width of 0.05 eV was used to improve convergence of states near the Fermi level. The Brillouin zone was sampled at the Gamma point. Optimized structures were obtained by minimizing the forces on each ion until they were less than 0.05 eV/Å.

Transition states (TSs) were located using the climbing-image nudged elastic band (CI-NEB) method.[5] The energy barrier ($E_{bar}$) was determined by calculating the energy difference between the corresponding transition state and initial state.

## 4. Catalytic results

The influence of activation gas in the FTS reaction over 10Fe0.8K/SiC catalyst is summarized in Table S5. The $H_2$ activation leads to the highest catalytic activity (57.3% of the CO conversion). The $CO/H_2$ (molar ratio at 1:1) activation with same conditions results in the lowest catalytic activity of 25.1% in CO conversion. The pure CO activation did not change the catalytic activity and product selectivity significantly compared to that in $H_2$. In contrast, a two-stage activation with firstly reduced in $H_2$ and then followed by pure CO activation gave a lower activity in the CO conversion of 45.7% with a slight decrease in the O/(O+P) as shown in Table S5.

Fig. S4 shows the time on stream (TOS) of CO conversion on the 10Fe0.8K/SiC catalyst activated in different gas. One can see that a higher initial CO conversion at about 20% was obtained

in $H_2$ activation relative to other gas activation (about 10%). It takes shorter time to attain stable stage with $H_2$ activation. However, the CO activation results in a slower increase in the CO conversion till the end of FTS reaction. The $H_2$/CO activation indicates a more stable but the lowest CO conversion.

## 5. Supplementary Figures and Tables

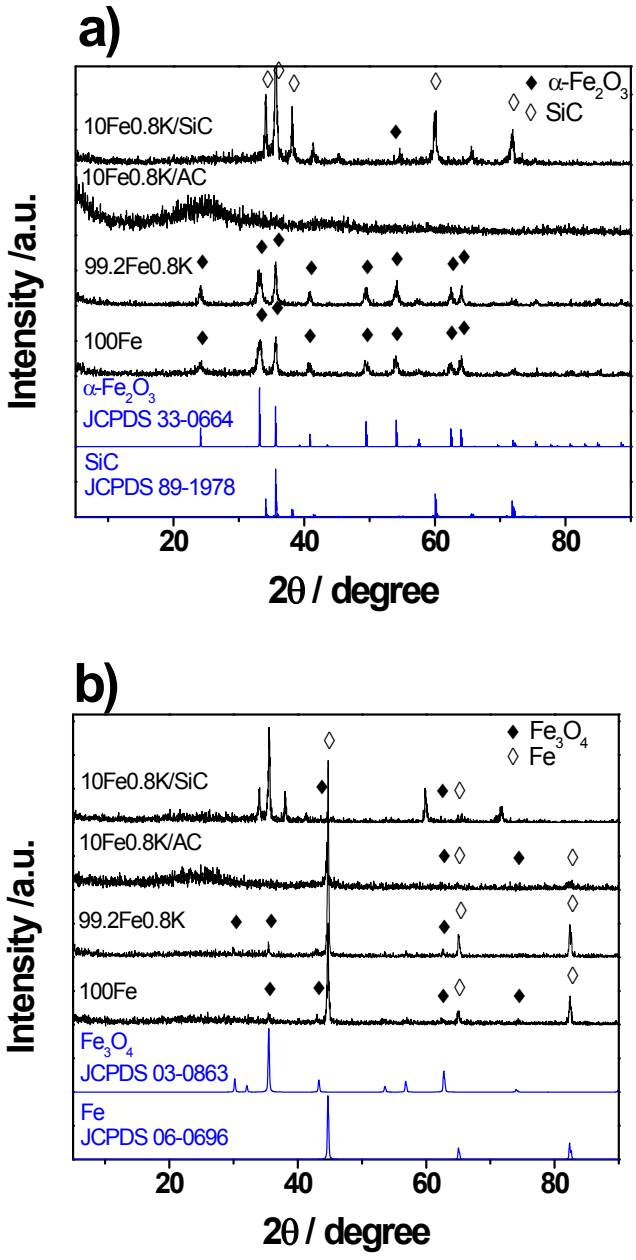

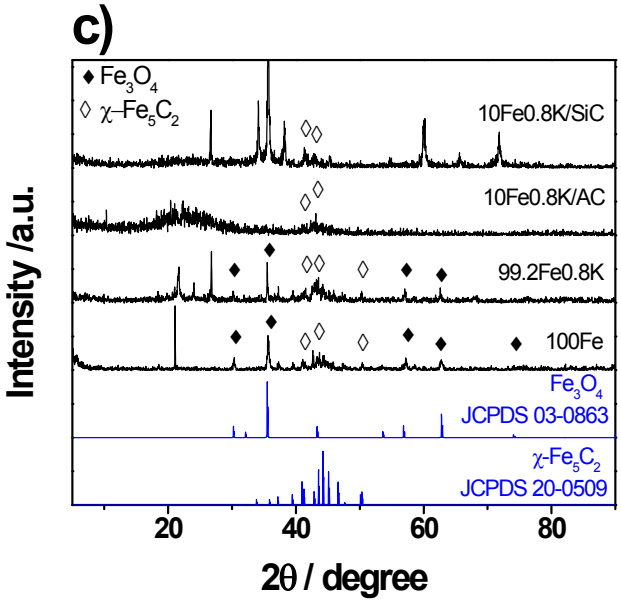


**Fig. S1** XRD patterns of the K-promoted iron catalysts after (a) calcination, (b) reduction and (c) reaction for 50 h.

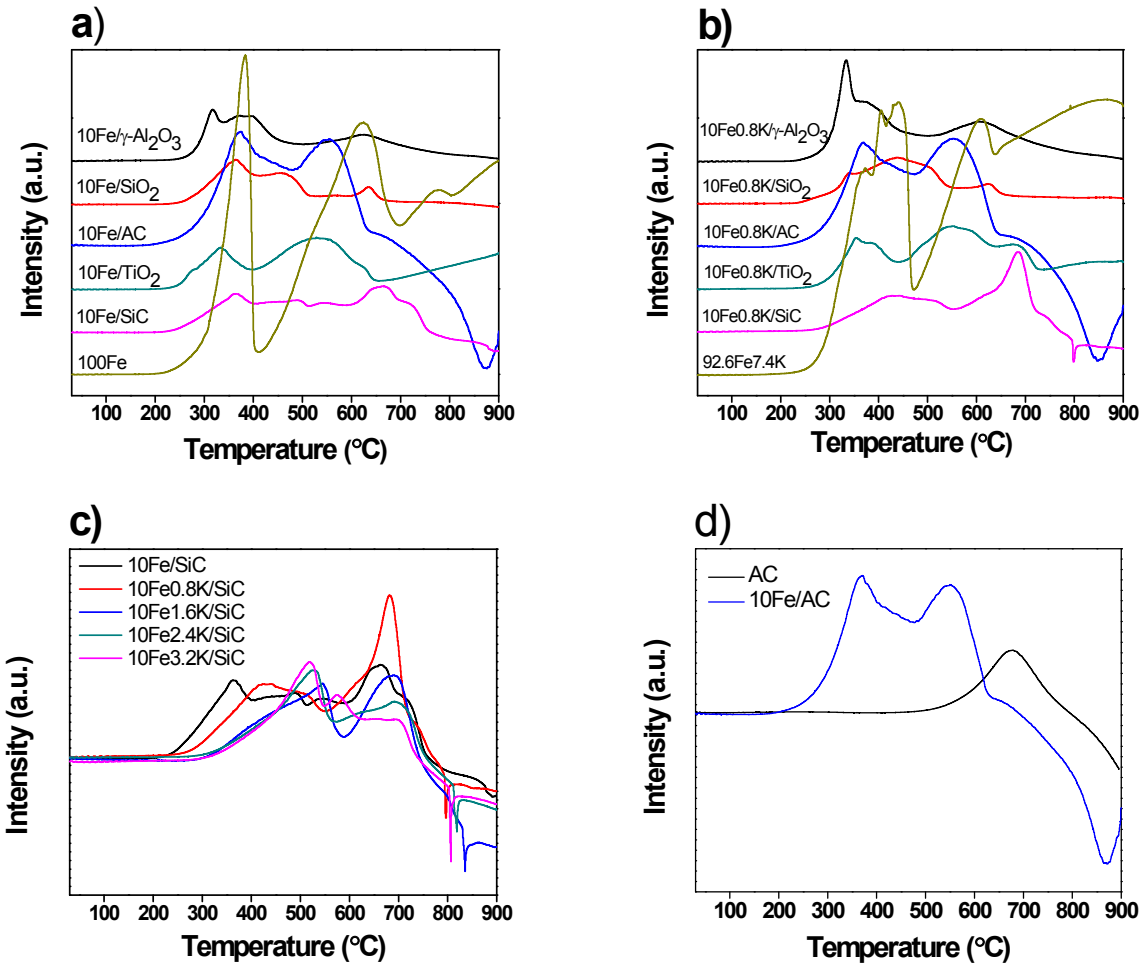

**Fig. S2** $H_2$TPR curves of various (a) unpromoted, (b, c) K-promoted iron catalysts, and (d) AC supported iron catalyst.

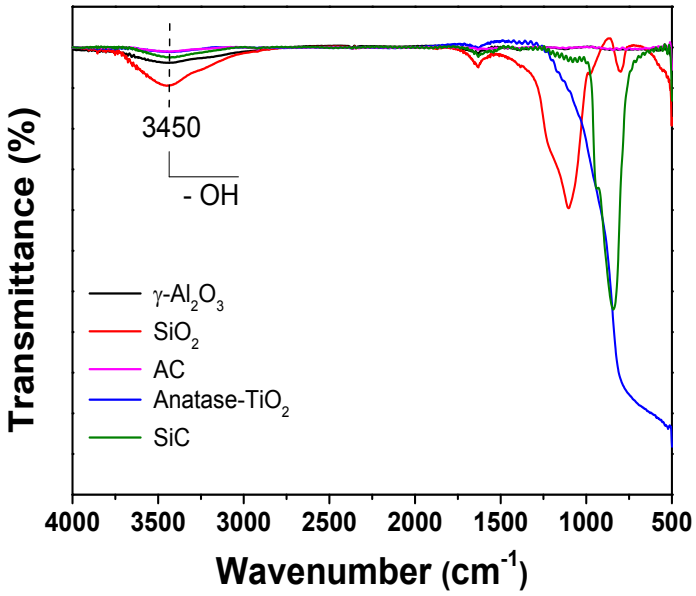


**Fig. S3** FTIR spectra of various supports measured after drying at 120 °C for 2 h.

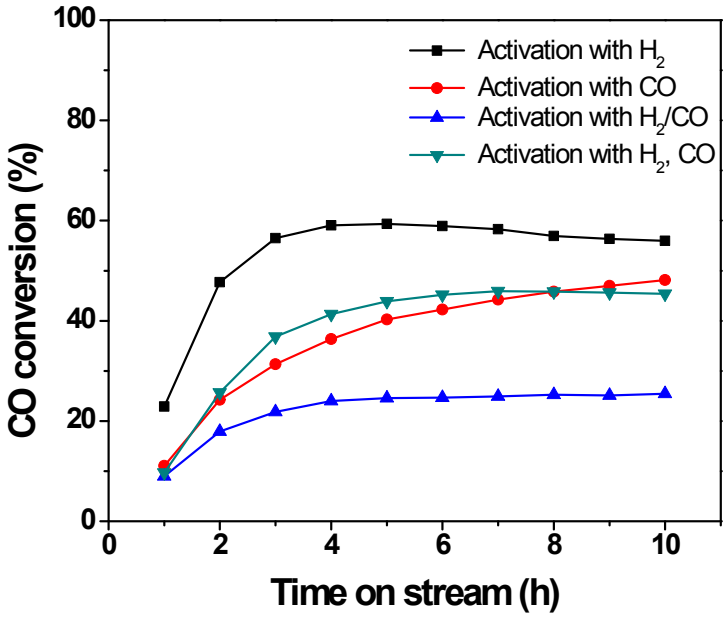


**Fig. S4** Time on stream of CO conversion for 10Fe0.8K/SiC catalyst activated in different gas and reacted under the conditions as described in Table S5.

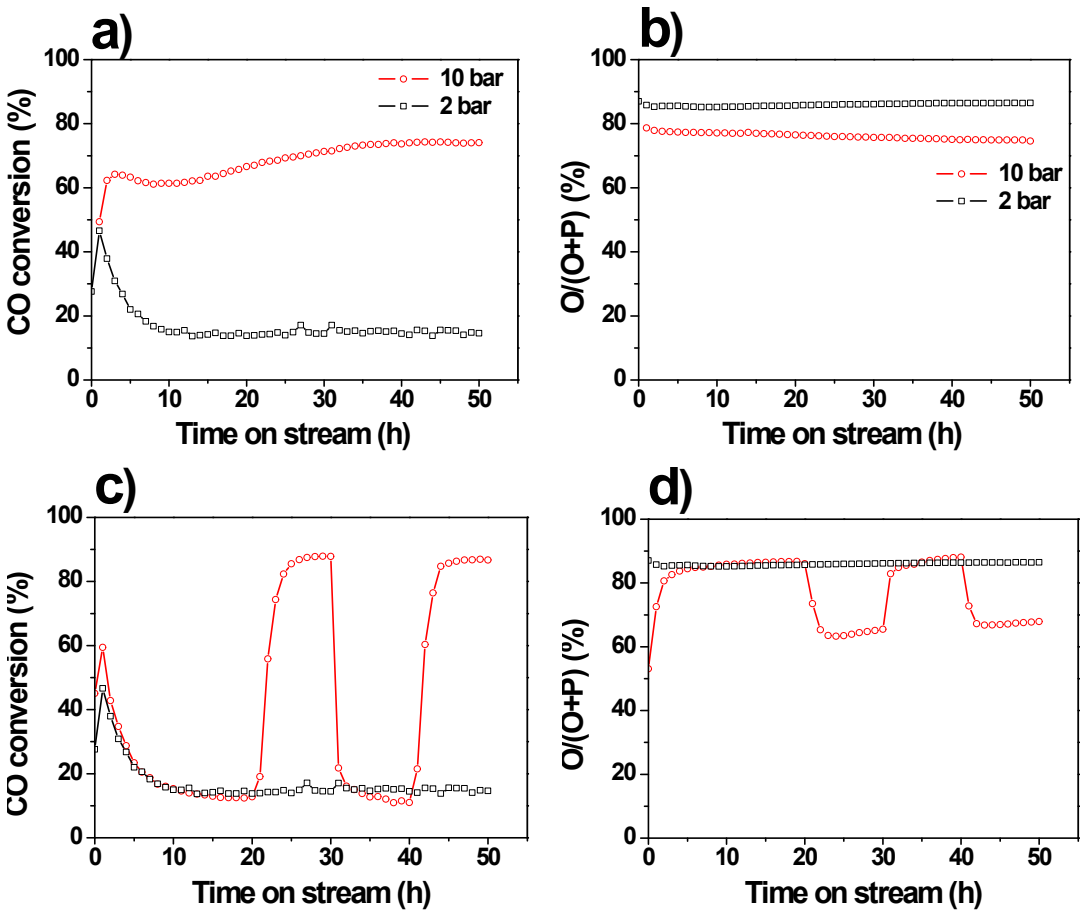


**Fig. S5** Time on stream of CO conversion and O/(O+P) in $C_2$-$C_4$ range over 10Fe0.8K/SiC catalyst under different reaction pressures. Reaction conditions: (1) for a) and b): $H_2/CO$ = 1.1; 300 °C; 10 bar and 2200 ml $g^{-1}$ $h^{-1}$ (red line); 2 bar and 733 ml $g^{-1}$ $h^{-1}$ (black line). (2) for c) and d): $H_2/CO$ = 1.1; 300 °C; 733 ml $g^{-1}$ $h^{-1}$; red line: 0-20 h and 30-40 h, 2 bar; 20-30 h and 40-50 h, 10 bar; black line: 0-50 h, 2 bar.

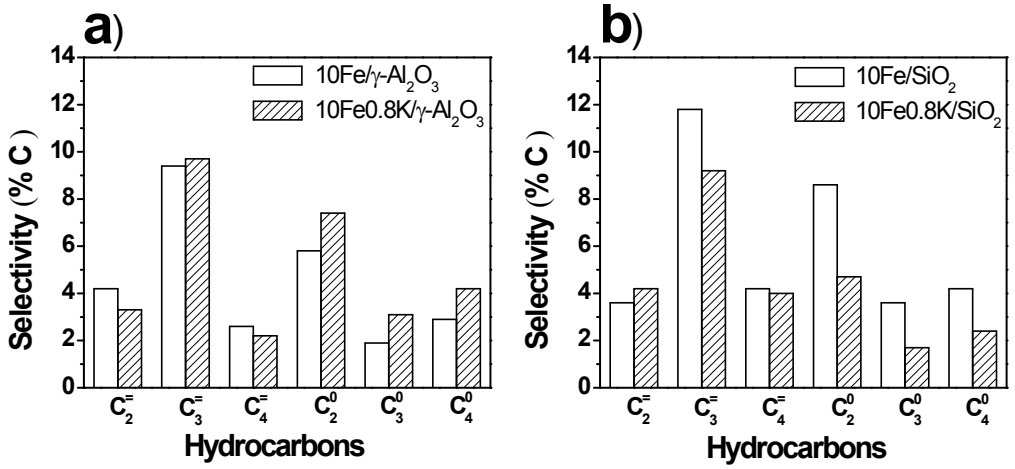

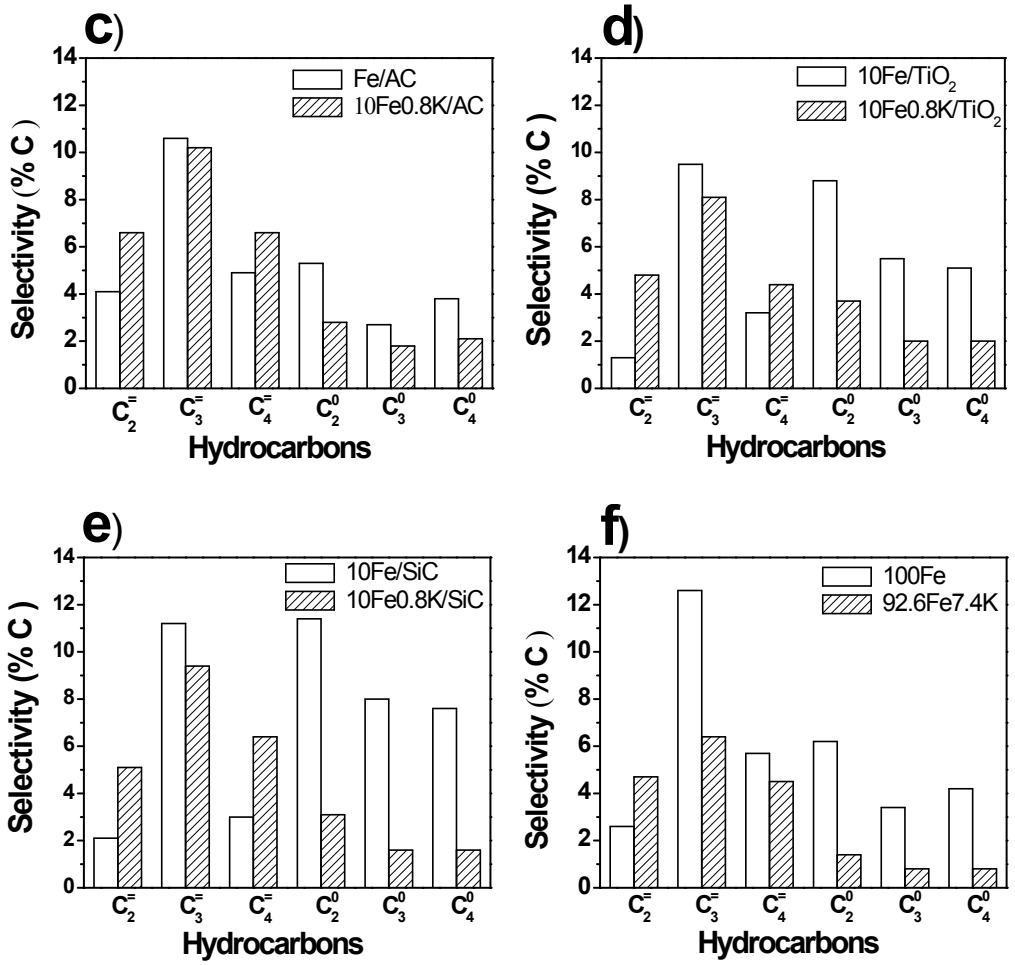


**Fig. S6** Comparison of $C_2$-$C_4$ range hydrocarbon selectivity between unpromoted and K-promoted iron catalysts on various supports under the conditions same as shown in Table 3.

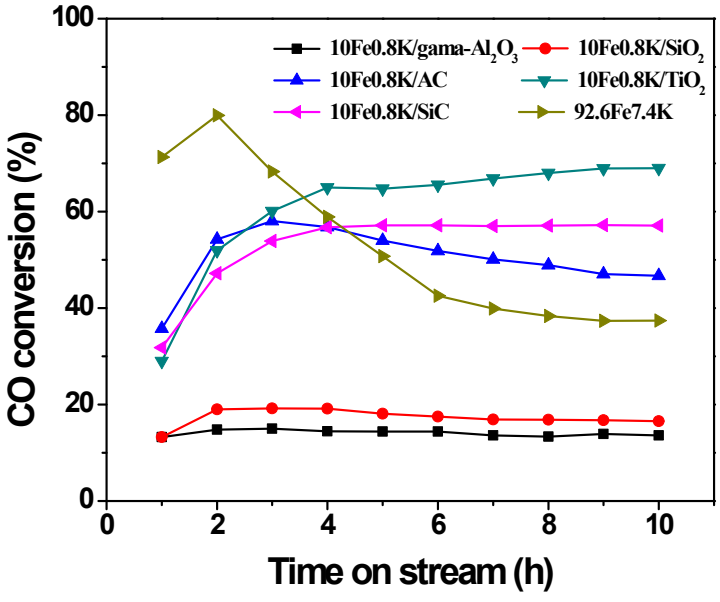

**Fig. S7** CO conversion versus time on stream for various K-promoted catalysts. Reaction conditions are the same as in Table 3.

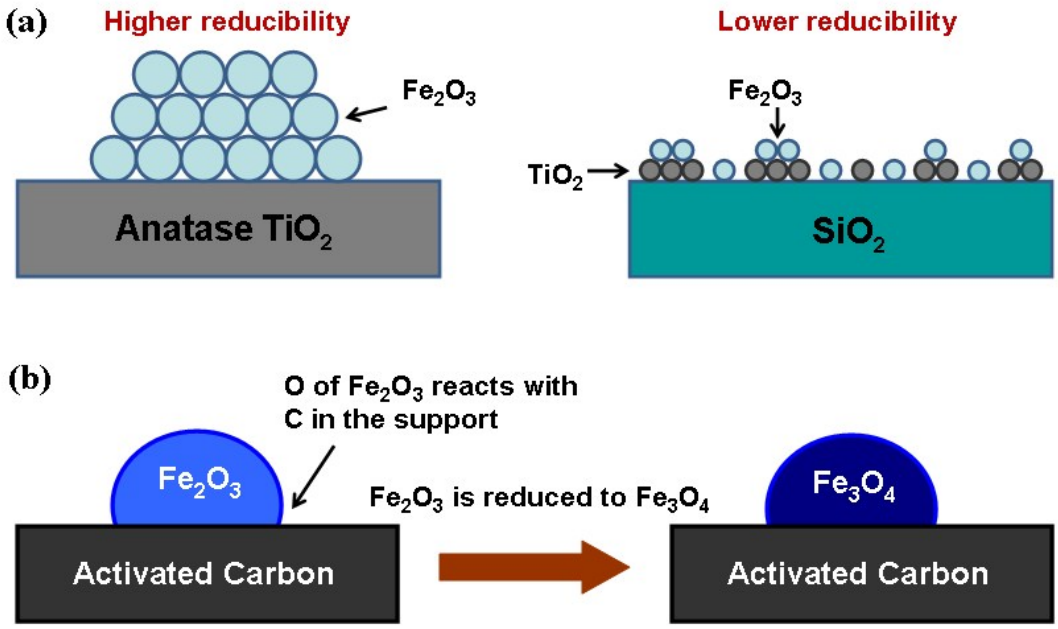


**Fig. S8** Schematic illustration of (a) favorable reduction of the larger porous α-$Fe_2O_3$ clusters on the anatase-$TiO_2$, and (b) α-$Fe_2O_3$ reduced to $Fe_3O_4$ by activated carbon.

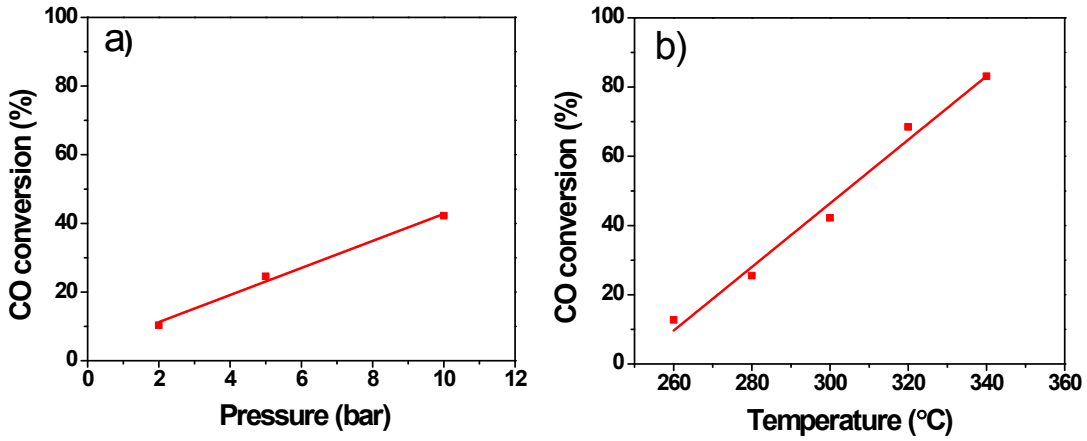


**Fig. S9** Plot of CO conversion as a function of the reaction pressure (a) and reaction temperature (b) over the 10Fe0.8Na0.1S/SiC catalyst under the conditions shown in Tables 5 and 6.

**Table S1.** Properties of different supports used for the preparation of iron-based catalysts

| Supports | Pore size (nm) | Pore volume ($cm^3\ g^{-1}$) | BET surface area ($m^2\ g^{-1}$) |
|---|---|---|---|
| $\gamma$-$Al_2O_3$ | 8.1 | 0.42 | 208.9 |
| $SiO_2$ (1) | 25.1 | 1.17 | 186.8 |
| $SiO_2$ (2) | 49.4 | 0.79 | 63.9 |
| AC | 1.9 | 0.39 | 810.8 |
| $TiO_2$ | 18.9 | 0.06 | 12.9 |
| SiC | 17.1 | 0.03 | 8.1 |

**Table S2.** Properties of iron-based catalysts with K promoted supported and precipitated iron-based catalysts

| Catalysts | Pore size (nm) | $Fe_2O_3$ size from TEM (nm) | Pore volume ($cm^3\ g^{-1}$) | BET surface area ($m^2\ g^{-1}$) |
|---|---|---|---|---|
| 10Fe0.8K/$\gamma$-$Al_2O_3$ | 7.0 | 1.74 | 0.35 | 197.2 |
| 10Fe0.8K/$SiO_2$ | 22.1 | 1.74 | 0.97 | 174.9 |
| 10Fe0.8K/AC | 1.9 | 1.07 | 0.31 | 639.6 |
| 10Fe0.8K/$TiO_2$ | 15.4 | 5.08 | 0.08 | 21.0 |
| 10Fe0.8K/SiC | 9.8 | 1.60 | 0.08 | 31.8 |
| 92.6Fe7.4K | 15.9 | 11.6 | 0.16 | 40.7 |

**Table S3.** Catalytic performance of alkali metal-promoted iron catalysts supported on SiC.[a]

| Catalysts | $X_{co}$ (%) | $CO_2$ selectivity (%) | CH selectivity (%C mol) | | | | O/(O+P) |
|---|---|---|---|---|---|---|---|
| | | | $CH_4$ | $C_2$−$C_4$ olefins | $C_2$−$C_4$ paraffins | $C_{5+}$ | |
| 10Fe/SiC | 26.6 | 24.4 | 17.3 | 16.1 | 26.7 | 39.8 | 37.6 |
| 10Fe0.8Li/SiC | 24.0 | 26.6 | 13.0 | 25.2 | 8.1 | 53.7 | 75.6 |
| 10Fe0.8Na/SiC | 31.3 | 38.8 | 9.2 | 18.7 | 4.9 | 67.2 | 79.3 |
| 10Fe0.8K/SiC | 57.1 | 43.5 | 10.0 | 19.7 | 5.8 | 64.5 | 77.1 |
| 10Fe0.8Rb/SiC | 56.3 | 43.6 | 13.9 | 22.6 | 7.8 | 55.7 | 74.4 |
| 10Fe0.8Cs/SiC | 46.7 | 43.4 | 12.9 | 22.0 | 7.5 | 57.7 | 74.6 |

[a] Reaction conditions: catalyst = 1.0 g , $H_2/CO$ = 1.1, GHSV = 2200 ml $g^{-1}$ $h^{-1}$, 300 °C, 10 bar, 10 h.

**Table S4.** Catalytic performance of the iron catalysts supported on SiC with different K loading.[a]

| Catalysts | $X_{co}$ (%) | $CO_2$ selectivity (%) | CH selectivity (%C mol) | | | | O/(O+P) |
|---|---|---|---|---|---|---|---|
| | | | $CH_4$ | $C_2$−$C_4$ olefins | $C_2$−$C_4$ paraffins | $C_{5+}$ | |
| 10Fe/SiC | 26.6 | 24.4 | 17.3 | 16.1 | 26.7 | 39.8 | 37.6 |
| 10Fe0.8K/SiC | 57.1 | 43.5 | 10.0 | 19.7 | 5.8 | 64.5 | 77.1 |
| 10Fe1.6K/SiC | 54.9 | 44.7 | 7.3 | 12.4 | 2.9 | 77.3 | 80.9 |
| 10Fe2.4K/SiC | 48.3 | 43.9 | 8.0 | 14.2 | 3.3 | 74.5 | 81.2 |

| | | | | | | | |
|---|---|---|---|---|---|---|---|
| 10Fe3.2K/SiC | 40.0 | 46.2 | 9.7 | 16.8 | 4.0 | 69.5 | 80.7 |

[a] Reaction conditions: catalyst = 1.0 g , $H_2/CO$ = 1.1, GHSV = 2200 ml $g^{-1}$ $h^{-1}$, 300 °C, 10 bar, 10 h.

**Table S5.** Effect of activation gas on the catalytic performance of 10Fe0.8K/SiC.[a]

| Activation gas | $X_{co}$ (%) | $CO_2$ selectivity (%) | CH selectivity (%C mol) | | | | O/(O+P) |
|---|---|---|---|---|---|---|---|
| | | | $CH_4$ | $C_2$−$C_4$ olefins | $C_2$−$C_4$ paraffins | $C_{5+}$ | |
| $H_2$ | 57.3 | 43.9 | 7.3 | 18.7 | 3.9 | 70.1 | 82.8 |
| CO | 50.8 | 40.7 | 7.1 | 17.0 | 3.4 | 72.6 | 83.5 |
| $H_2/CO$ [b] | 25.1 | 33.4 | 7.6 | 16.6 | 2.9 | 72.9 | 84.9 |
| $H_2$, CO[c] | 45.7 | 42.0 | 6.3 | 12.9 | 3.5 | 77.3 | 78.9 |

[a] Reaction conditions: catalyst = 1.0 g, $H_2/CO$ = 1.1, GHSV = 2200 ml $g^{-1}$ $h^{-1}$, 300 °C, 10 bar, 10 h. [b] Molar ratio of $H_2/CO$ =1. [c] Firstly reduced with $H_2$, and then switch to CO at 350 °C for 3 h.

**Table S6.** Effect of reaction temperature on the catalytic performance of 10Fe0.8K/SiC.[a]

| Reaction temperature (°C) | $X_{co}$ (%) | $CO_2$ selectivity (%) | CH selectivity (%C mol) | | | | O/(O+P) |
|---|---|---|---|---|---|---|---|
| | | | $CH_4$ | $C_2$−$C_4$ olefins | $C_2$−$C_4$ paraffins | $C_{5+}$ | |
| 300 | 40.9 | 45.9 | 10.6 | 23.5 | 5.9 | 60.0 | 80.1 |
| 320 | 72.9 | 47.4 | 14.1 | 23.7 | 6.9 | 55.3 | 77.3 |
| 340 | 75.9 | 46.8 | 15.5 | 23.6 | 7.5 | 53.3 | 75.9 |

[a] Reaction conditions: catalyst = 1.0 g, $H_2/CO$ = 1.1, GHSV = 2200 ml $g^{-1}$ $h^{-1}$, 10 bar, 10 h.

**Table S7.** Effect of reaction pressure on the catalytic performance of 10Fe0.8K/SiC.[a]

| Reaction pressure (bar) | $X_{co}$ (%) | $CO_2$ selectivity (%) | CH selectivity (%C mol) | | | | O/(O+P) |
|---|---|---|---|---|---|---|---|
| | | | $CH_4$ | $C_2$−$C_4$ olefins | $C_2$−$C_4$ paraffins | $C_{5+}$ | |
| 2 | 11.1 | 46.4 | 19.1 | 34.8 | 4.8 | 41.3 | 87.8 |
| 5 | 34.7 | 44.2 | 14.0 | 25.6 | 5.4 | 55.0 | 82.6 |
| 10 | 57.1 | 43.5 | 9.6 | 19.1 | 5.2 | 66.1 | 78.6 |

[a] Reaction conditions: catalyst = 1.0 g, $H_2/CO$ = 1.1, GHSV = 2200 ml $g^{-1}$ $h^{-1}$, 300 °C, 10 h.

**Table S8.** Olefin distribution in the $C_2$-$C_4$ hydrocarbons over S-promoted iron catalysts.[a]

| Catalysts | T (°C) | $X_{co}$ (%) | $C_2$-$C_4$ olefins Selectivity (%) | Product distribution in $C_2$-$C_4$ hydrocarbons | | | | | |
|---|---|---|---|---|---|---|---|---|---|
| | | | | $C_2^=$ | $C_2^0$ | $C_3^=$ | $C_3^0$ | $C_4^=$ | $C_4^0$ |
| 10Fe3.2Na0.1S/SiC | 300 | 18.2 | 23.9 | 30.0 | 7.2 | 33.8 | 4.1 | 21.0 | 3.9 |
| 10Fe3.2K0.1S/6$CSiO_2$[b] | 320 | 32.1 | 39.7 | 20.8 | 12.7 | 37.6 | 4.7 | 17.1 | 7.1 |
| 10Fe3.2K0.1S/6$CSiO_2$[c] | 300 | 29.3 | 35.8 | 22.6 | 8.5 | 37.7 | 3.9 | 22.0 | 5.3 |
| 10Fe3.2K0.1S/6$CSiO_2$[c] | 320 | 60.6 | 33.9 | 18.6 | 13.5 | 38.0 | 5.1 | 18.2 | 6.6 |
| 30Fe3.2K0.6S/6$CSiO_2$[c] | 300 | 12.1 | 47.7 | 29.4 | 5.7 | 36.9 | 3.2 | 20.8 | 4.0 |

| | | | | | | | | | |
|---|---|---|---|---|---|---|---|---|---|
| 30Fe3.2K0.6S/6C$SiO_2$[c] | 320 | 38.3 | 36.5 | 29.2 | 7.9 | 36.5 | 3.3 | 19.1 | 4.0 |

[a] Reaction conditions: catalyst = 1.0 g, $H_2$/CO = 1.1, GHSV = 2200 ml $g^{-1}$ $h^{-1}$,10 bar, 10 h. [b] support pore size = 25.1 nm. [c] support pore size = 49.4 nm.

## References:


1. G. Kresse, and J. Furthmuller, *Phys. Rev. B,* 1996, ***54***, 11169-11186.
2. G. Kresse and J. Furthmuller, *Comput. Mater. Sci.*, 1996, ***6***, 15-50.
3. P.E. Bllöchl, *Phys. Rev. B,* 1994, ***50***, 17953-17979.
4. J.P. Perdew, K. Burke and M. Ernzerhof, *Phys. Rev. Lett.* 1996, ***77***, 3865-3868.
5. G. Henkelman, B.P. Uberuaga and H. Jonsson, *J. Chem. Phys.* 2000, ***113***, 9901–9904.